Review of Scientific Instruments

ECRIS plasma spectroscopy with a high resolution spectrometer

Cite as: Rev. Sci. Instrum. **91**, 013318 (2020); https://doi.org/10.1063/1.5128854
Submitted: 23 September 2019 . Accepted: 26 December 2019 . Published Online: 17 January 2020

R. Kronholm, T. Kalvas, H. Koivisto, S. Kosonen, M. Marttinen, D. Neben, M. Sakildien, O. Tarvainen, and V. Toivanen

Review of Scientific Instruments ARTICLE scitation.org/journal/rsi

ECRIS plasma spectroscopy with a high resolution spectrometer

Cite as: Rev. Sci. Instrum. 91, 013318 (2020); doi: 10.1063/1.5128854
Submitted: 23 September 2019 • Accepted: 26 December 2019 •
Published Online: 17 January 2020

R. Kronholm,[1,a)] T. Kalvas,[1] H. Koivisto,[1] S. Kosonen,[1] M. Marttinen,[1] D. Neben,[2] M. Sakildien,[3] O. Tarvainen,[4] and V. Toivanen[1]

AFFILIATIONS

[1]Department of Physics, University of Jyväskylä, 40500 Jyväskylä, Finland
[2]National Superconducting Cyclotron Laboratory, Michigan State University, East Lansing, Michigan 48824, USA
[3]iThemba LABS, P.O. Box 722, Somerset West 7131, South Africa
[4]UK Research and Innovation, STFC Rutherford Appleton Laboratory, Chilton OX11 0QX, United Kingdom

Note: Invited paper, published as part of the Proceedings of the 18th International Conference on Ion Sources, Lanzhou, China, September 2019.
[a)]**Electronic mail:** risto.j.kronholm@jyu.fi

ABSTRACT

Electron Cyclotron Resonance Ion Source (ECRIS) plasmas contain high-energy electrons and highly charged ions implying that only non-invasive methods such as optical emission spectroscopy are reliable in their characterization. A high-resolution spectrometer (10 pm FWHM at 632 nm) enabling the detection of weak emission lines has been developed at University of Jyväskylä, Department of Physics (JYFL) for this purpose. Diagnostics results probing the densities of ions, neutral atoms, and the temperature of the cold electron population in the JYFL 14 GHz ECRIS are described. For example, it has been observed that the cold electron temperature drops from 40 eV to 20 eV when the extraction voltage of the ion source is switched off, accompanied by two orders of magnitude decrease in Ar^{9+} optical emission intensity, suggesting that diagnostics results of ECRIS plasmas obtained without the extraction voltage are not depicting the plasma conditions of normal ECRIS operation. The relative changes of the plasma optical emission and the ion beam current have been measured in CW and amplitude modulation operation mode of microwave injection. It is concluded that in the CW mode, the ion currents could be limited by diffusion transport and electrostatic confinement of the ions rather than beam formation in the extraction region and subsequent transport. The high resolution of the spectrometer allows determining the ion temperature by measuring the Doppler broadening of the emission lines and subtracting the wavelength dependent instrumental broadening. The measured ion temperatures in the JYFL 14 GHz ECRIS are between 5 and 28 eV, depending on the plasma species and charge state. Gas mixing is shown to be an effective method to decrease the ion temperature of high charge state argon ions from 20 eV in pure argon discharge to 5 eV when mixed with oxygen.

I. INTRODUCTION

Diagnostics of Electron Cyclotron Resonance Ion Source (ECRIS) plasmas characterized by a strong external magnetic field and the presence of high-energy electrons and highly charged ions are challenging. The sensitivity of the plasma conditions for external disturbances imply that only noninvasive methods such as optical emission spectroscopy (OES) can be applied[1–3] to investigate their properties such as electron energies, densities of neutral particles and ions, reaction rates, and ion temperatures. The high charge state ion densities and the intensities of the respective emission lines are often extremely low, which sets requirements for the sensitivity of the OES setup. The measurement of the ion temperature requires outstanding wavelength resolution and appropriate understanding of the line broadening mechanisms including instrumental effects. Only few OES studies have been conducted with high-frequency ECR ion sources.[4–7] We review OES studies conducted with a 14 GHz ECRIS[8] and present new data supplementing the previously reported results.[1–3] Recent improvements of the high resolution spectrometer are described and technical aspects of future requirements are discussed.

TABLE I. Specifications of the monochromator.

Optics configuration	Fastie-Ebert
Focal length	996 mm
Diffraction grating	Holographic 2200 grooves/mm
Wavelength range	300–800 nm
Input and output slits	Adjustable 10–100 μm
Numerical aperture	0.05
Geometrical extent	0.001 with high resolution slits
Theoritical Resolving power	200 000
Real resolving power	165 000 at 488 nm
Resolution FWHM	12 pm at 488 nm
Photomultiplier	ETEnterprises 9816B
Data acquisition	Phase-sensitive frequency lock-in
Lock-in frequency	10–10 000 Hz

II. THE EXPERIMENTAL SETUP

The spectrometer consists of an optical interface and coupling system connected to the ECRIS offering a line-of-sight view through the plasma, a high-resolution monochromator and a photomultiplier tube connected to a phase-locking data acquisition system improving the signal-to-noise ratio. The specifications of the Fastie-Ebert type monochromator are listed in Table I with the measurement schematic shown in Fig. 1(a). A detailed description of the system (with figures) is reported elsewhere.[1]

The setup allows resolving the emission lines of ions and neutral particles and determining their intensities and linewidths. The spectrometer resolution allows measuring the Doppler broadening of the emission lines yielding the corresponding ion temperatures. It is imperative to know the wavelength-dependent instrumental broadening of the device. This is because (a) the instrumental broadening must be subtracted when studying the Doppler broadening and (b) the measurement of line emission intensities requires integrating across the emission line rather than simply monitoring the peak of the emission line as the instrumental and physical broadenings are comparable. The instrumental broadening (FWHM) of the setup as a function of the measured wavelength can be calculated (in nanometer) from

$$\Delta\lambda_{\mathrm{FWHM}} = \frac{d\lambda}{dx}\cdot w = \frac{10^6\cos\beta}{knL}\cdot w, \tag{1}$$

where $d\lambda/dx$ is the linear dispersion, w is the width of the exit slit in millimeter, k is the diffraction order, n is the groove density (grooves/millimeter), L is the exit arm length in millimeter, and β is the angle of diffraction in radians.[3] The instrumental broadening calculated from Eq. (1) was confirmed by measuring the well-known narrow linewidths of three lasers with 100 μm and 10 μm slits: HeNe at 632 nm, diode-pumped frequency-doubled single-mode laser at 532 nm and argon ion laser at 458, 488, and 514 nm. The results are summarized in Table II.

The spectrometer has been recently upgraded by changing the monochromator entrance and exit slits from linear to circular, which minimizes the astigmatism of the optics.[9] The astigmatism correction has allowed to double the slit width from 10 μm (linear slits) to 20 μm (circular slits) without compromising the 13.2 pm resolution at 488 nm while increasing the throughput of the monochromator. Removing the astigmatism mitigates the complexity of linewidth data analysis by canceling the inevitable asymmetry due to imperfect optical matching from the linear slits to the spherical mirror as shown in Fig. 1(b). Altogether, this allows detecting weaker emission lines and measuring their broadening at the total resolution reported in Table I without prolonging the measurement time (approximately

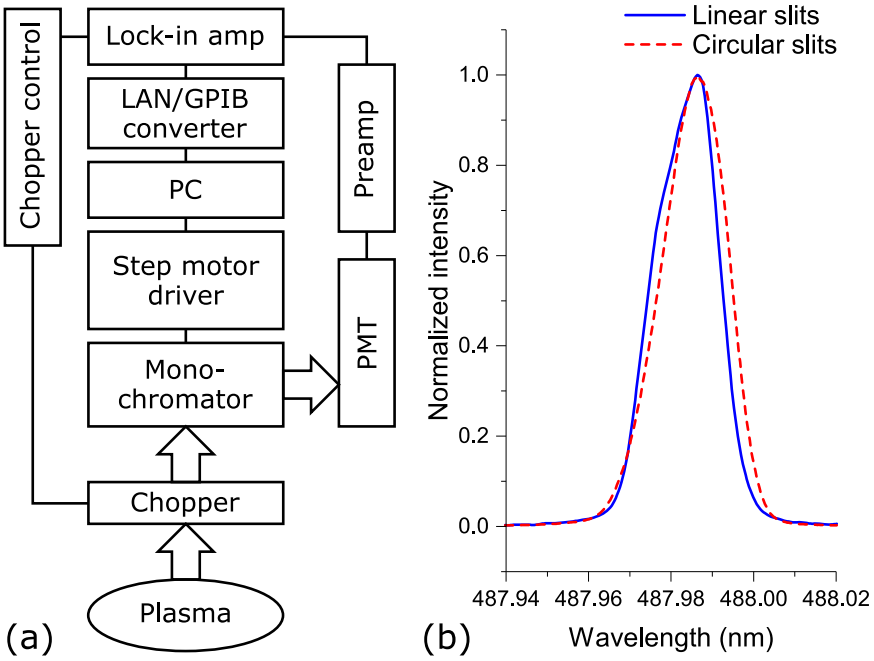

FIG. 1. (a) A schematic of the measurement setup. The light path is indicated with arrows and signal paths with lines. (b) The instrumental profile of argon ion laser emission line at 488 nm measured with circular and linear slits. The asymmetry observed with the linear slits is a sign of astigmatism.

TABLE II. Comparison of the calculated and measured instrumental broadening of the Fastie-Ebert monochromator.

Wavelength (nm) (laser)	Calculated $\Delta\lambda$ (pm)	Measured $\Delta\lambda$ (pm)
100 μm slit		
458	38	39.5
488	36.9	36.5
514	36	36.2
632	30.7	30.7
10 μm slit		
532	11.5	11.5
632	9.8	9.8

10 min/line). The prospects of the upgraded setup are discussed in Sec. IV.

III. EXPERIMENTAL RESULTS

A. The temperature of the cold electron population

The temperature T_e of the electron population can be studied by comparing the measured emission line intensities to the excitation rates from the same lower energy state (most often the ground state) to different excited states j and k. The excitation cross sections should have different electron energy dependencies for reliable results. The observed emission intensities can be connected to the T_e-dependent rate coefficients, calculated from the cross sections assuming a certain electron energy distribution (EED), through

$$\frac{I_j}{I_k} = \frac{n_e n_q \langle \sigma_j v_e \rangle BR_j}{n_e n_q \langle \sigma_k v_e \rangle BR_k} = \frac{\langle \sigma_j v_e \rangle BR_j}{\langle \sigma_k v_e \rangle BR_k}, \quad (2)$$

where n_e and n_q are the densities of electrons and ions (or neutrals), $\langle \sigma v_e \rangle$ is the rate coefficient of the electron impact reaction, and BR the branching ratio of the observed emission line.[1] The reliability of the analysis can be increased by comparing the ratios of multiple emission lines, which in practice limits the use of the method to probing the temperature of the cold electron population of the ECRIS plasma, which predominantly excite and ionize neutral particles and low charge state ions. This is because the emission lines of high charge state ions are often either too weak to be detected or are outside the detectable wavelength range. If the observed transitions j and k originate from different charge states q_1 and q_2 and the electron temperature can be deduced as described above, the ratio of the densities of these charge states can be estimated.

The line-ratio method has been applied for estimating the cold electron temperature in a neon discharge of the JYFL 14 GHz ECRIS.[1] Since the actual EED of the cold electrons is unknown, the temperature was estimated for Maxwellian and Druyvesteyn distributions, both commonly used for describing laboratory plasmas. The cold electron temperature was found to change significantly when the extraction voltage is turned on/off. The results are summarized in Table III.

Switching off the extraction voltage decreases the average energy of the cold electron population. The absolute emission intensity of all observed transitions was also higher despite the lower cold electron temperature (at constant gas feed rate). This implies that the high voltage influences the charge state distribution and ion dynamics, presumably due to the so-called ion pumping effect as the extraction process can be considered as an ion sink affecting the loss rates and densities of charged particles. The conclusion is supported by observing the Ar^{9+} emission line (at 553.3265 nm) intensity decreasing approximately by a factor of 50 when the high voltage is switched off. These findings underline the importance of performing ECRIS plasma diagnostics under conditions relevant for the ion source operation, i.e., with the extraction voltage applied.

TABLE III. The effect of high voltage on the cold electron temperature and average energy (Maxwell and Druyvesteyn EED) of a neon plasma in the JYFL 14 GHz ECRIS.

	Maxwellian	Druyvesteyn
$f(\epsilon) = \langle E_e \rangle^{-3/2} \alpha e^{\frac{-\epsilon\beta}{\langle E_e \rangle}}$		
α	$\frac{\Gamma(5/2)^{3/2}}{\Gamma(3/2)^{5/2}}$	$\frac{\Gamma(5/4)^{3/2}}{\Gamma(3/4)^{5/2}}$
β	$\frac{\Gamma(5/2)}{\Gamma(3/2)}$	$\frac{\Gamma(5/4)}{\Gamma(3/4)}$
HV ON		
$T_{e,cold}$ (eV)	40 ± 20	40 ± 20
$\langle E_{e,cold} \rangle$ (eV)	60 ± 30	60 ± 30
HV OFF		
$T_{e,cold}$ (eV)	20 ± 10	30 ± 20
$\langle E_{e,cold} \rangle$ (eV)	30 ± 15	45 ± 30

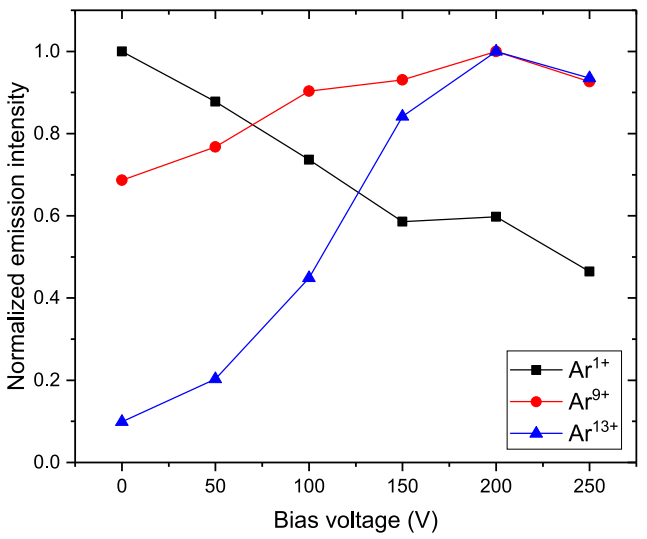

FIG. 2. The optical emission intensities of Ar^+, Ar^{9+}, and Ar^{13+} as a function of the biased disc voltage (negative with respect to the plasma chamber).

Since the effect of applying the extraction voltage is (to a certain degree) similar to applying a negative voltage on the biased disc,[10] the emission intensities of Ar^{+}, Ar^{9+}, and Ar^{13+} were measured as a function of the biased disc voltage. The results displayed in Fig. 2 support the view that regulating the axial electron and ion losses changes the charge state distribution drastically. With the disc connected to the plasma chamber, the Ar^{13+} emission intensity was only 10% of that observed at −200 V bias voltage. In contrast, the emission intensity of Ar^{+} was halved with increasing voltage. The biased disc is believed to influence the distribution of ion fluxes and hence the Charge State Distribution (CSD).[11] The presented comparison of the effects of the biased disc and the extraction voltage implies that they affect the CSD through similar mechanism.

B. Microwave power amplitude modulation

The correlation between high charge state ion densities and the extracted beam currents can be studied with OES.[2] In CW operation mode, the ion currents can be limited by diffusion transport and electrostatic confinement of the high charge state ions, implying that the extracted beam intensities could be improved by limiting the ion confinement time (of a certain charge state).

To corroborate this conclusion, the microwave power was amplitude modulated using a square waveform with varying modulation frequency and 50% duty factor producing fast transients between 200 W and 530 W output powers, simultaneously observing the beam currents and optical emission signals of Ar^{9+} (553.3265 nm) and Ar^{13+} (441.2556 nm). Figure 3 shows the result for Ar^{13+} with AM frequencies ranging from 7 Hz to 31 Hz.

With 7 Hz AM frequency [Fig. 3(a)], both the optical emission and beam current signals first saturate before an "afterglow" transient reaching 50 μA current is observed coinciding with the drop of power. The existence of the afterglow implies the existence of an ion population that can escape only when the electron heating rate is reduced, presumably affecting the electrostatic confinement of the ions. When the AM frequency is increased, the optical emission intensity of Ar^{13+} decreases (all optical signals are normalized to a common maximum) suggesting that the high-power state of the AM signal is not long enough to reach an equilibrium. At the same time, both the extracted beam current reached during the high-power state and the peak afterglow current decrease approximately by a factor of 2. The peak current of the afterglow transient is proportional to the optical emission signal, not to the beam current reached during the high-power state, i.e., the transient surge of ions escaping the confinement is proportional to the ion density in the discharge. This leads to the conclusion that the extracted ion current in CW mode is limited by electrostatic confinement trapping the ions. In the case of Ar^{9+}, the decrease of the afterglow signal was observed at higher AM frequency matching with the saturation of the optical emission signal (similar to Ar^{13+} shown here), which is consistent with the above qualitative description of the high charge state ion reservoir build-up.

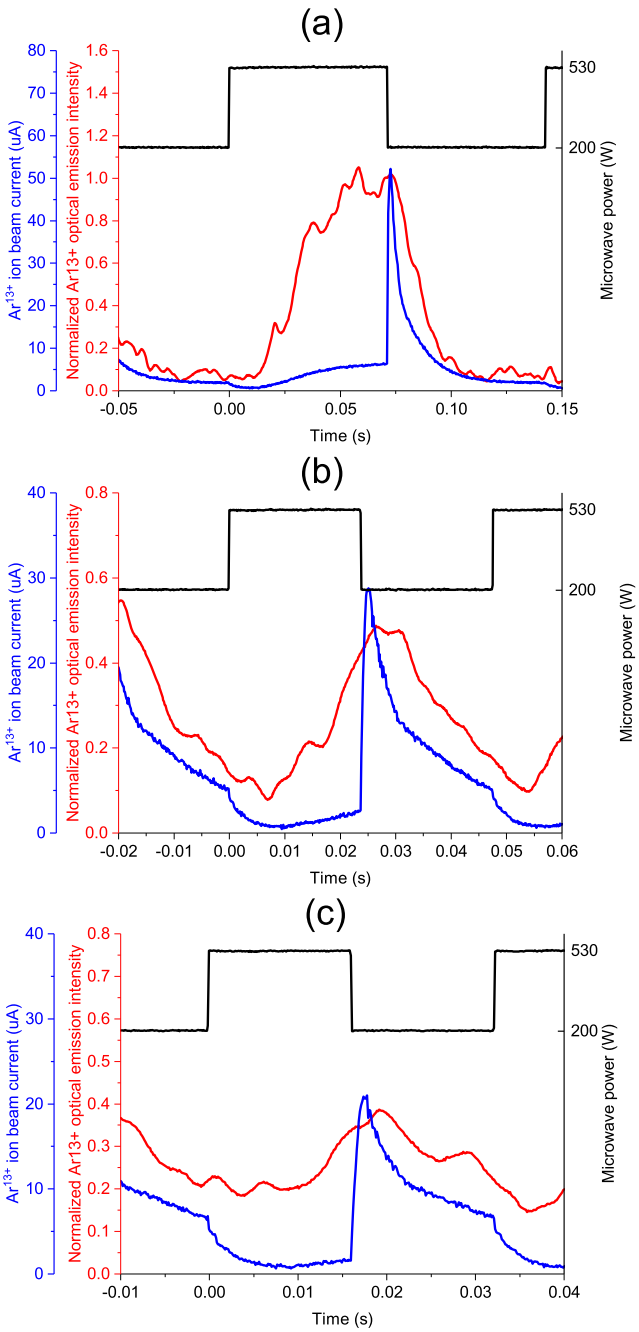

FIG. 3. The response of Ar^{13+} optical emission and beam current to amplitude modulation at (a) 7 Hz, (b) 21 Hz, and (c) 31 Hz with 50% duty factor. Notice that the axis scales change between the subfigures.

C. Ion temperature and the effect of gas mixing

The measured ion temperatures in single element discharge, i.e., without gas mixing, in the JYFL 14 GHz ECRIS are found to be between 5 and 28 eV, depending on the plasma species and the charge state as well as the ion source tune.[3] Table IV shows a summary of the ion temperatures. The argon ion temperatures of the confined ion population (probed by OES) are compared to those deduced from the energy spread of the extracted beams determined with a retarding field analyzer[12] and representing the effective ion temperature of the extracted ions.

TABLE IV. The average ion temperature obtained through OES and from the energy spread of the extracted beams (*N* samples measured at different source settings).

Ion/neutral species	OES T_i (eV) (N)	Beam $T_{i,eff}$ (eV) (N)
He^0	1 (12)	
He^+	6 (2)	
N^+	6 (4)	
N^{2+}	10 (3)	
N^{3+}	11 (2)	
Ne^0	5 (4)	
Ne^+	13 (7)	
Ar^0	5 (2)	
Ar^+	13 (25)	
Ar^{2+}	19 (5)	
Ar^{5+}		18 (4)
Ar^{6+}		19 (6)
Ar^{7+}		21 (6)
Ar^{8+}		21 (6)
Ar^{9+}	14 (28)	24 (6)
Ar^{10+}	14 (2)	26 (6)
Ar^{11+}		26 (6)
Ar^{12+}		27 (5)
Ar^{13+}	21 (47)	27 (5)
Ar^{14+}		28 (2)

The following conclusions have been drawn:[3] (i) the ion temperatures are significantly higher than conventionally considered for ECR plasmas[13,14] but agree well with those measured in a quadrupole fusion machine,[15,16] (ii) the ion temperature depends on the charge state, (iii) the optical data are in reasonably good agreement with the effective ion temperatures deduced from the energy spread of the beam, the latter seemingly overestimating the temperature of the confined ion population, and (iv) the 1+ ions are notably hot in comparison to neutral particles. Furthermore, it was observed that (v) optimizing the beam currents of high charge state argon ions corresponds to a drop in their temperatures.

Figure 4 shows the effect of gas mixing[17,18] on the ion temperature. The ion temperature in pure argon discharge increases with the charge state as reported earlier.[3] When the same emission lines of Ar^+, Ar^{9+}, and Ar^{13+} were measured with a small leak of air contaminating the gas in the feed line, and resulting in an argon-nitrogen mixture being injected into the ion source, the ion temperatures of the high charge state ions (Ar^{9+} and Ar^{13+}) were lower by several electronvolt. To confirm the result, the leak was eliminated and oxygen was fed into the plasma chamber from another gas inlet optimizing the mixing ratio of Ar and O_2 for Ar^{13+} production. In this case, the temperature of the high charge state Ar ions decreased from 16–20 eV to 5–7 eV. Interestingly, the Ar^+ temperature was hardly affected. Furthermore, it was observed that the temperature of the low charge state oxygen ions was approximately the same as the temperature of the high charge state argon ions.

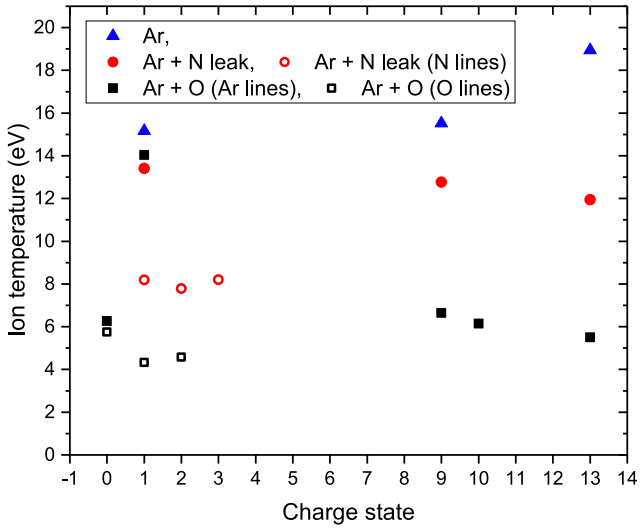

FIG. 4. The ion temperatures in discharges of pure argon, argon with a nitrogen leak, and argon with oxygen. In the first (Ar) and second (Ar + N_2 leak) case, the total pressure was optimized for Ar^{13+} beam production, whereas in the last case (Ar + O_2) both, the total pressure and the gas mixing ratio were optimized for Ar^{13+} beam production.

The result deviates from an earlier observation[19] suggesting that gas mixing has only a weak effect on the energy spread (effective temperature) and emittance of high charge state ions of the heavier constituent. The difference between the results obtained by probing the ion temperature in the plasma and from the extracted beam is most likely due to the fact that the extracted ions represent the part of the ion distribution escaping the electrostatic confinement, i.e., have a sufficient energy to overcome the potential barrier. Thus, the measurement of the energy spread of the extracted beam only accounts for those ions belonging to the tail of the confined ion energy distribution. This view is supported by the optical emission intensities and extracted charge state distributions for the pure argon and argon-oxygen mixtures, shown in Fig. 5. With the optimized mixing ratio, the argon feed rate is approximately 10% in comparison to the pure argon discharge. Nevertheless, the optical emission intensity of Ar^{13+} is approximately 4 times higher with the optimized gas mixing, indicating that the Ar^{13+} density in the plasma has increased dramatically. At the same time, the extracted beam current of Ar^{13+} has increased only by a factor of 1.5 in comparison to the pure argon discharge. The observation is consistent with electrostatic ion confinement in a local potential dip ($\Delta\Phi$), i.e., only those ions that have enough energy to overcome the potential barrier are extracted. Thus, it seems that gas mixing decreasing the temperature of high charge state ions increases their density in the plasma, while the beam current is still limited by the flux of ions escaping the confinement. Gas mixing could also affect the spatial distribution of the ambipolar plasma potential and, in particular, the value of $\Delta\Phi$. Further experiments with different mixing ratios and combinations of gases together with the measurement of the afterglow beam current transient, being an indicator of the confined ion reservoir, are required to draw quantitative conclusions.

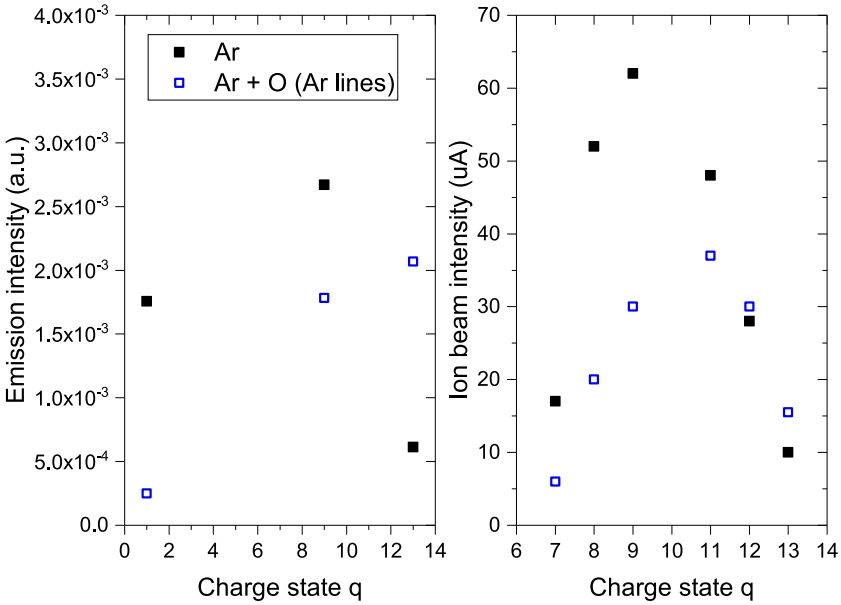

FIG. 5. The optical emission intensities of Ar^{+}, Ar^{9+}, and Ar^{13+} ions (left) and the charge state distribution of extracted argon ions (right) for the pure argon plasma and argon-oxygen plasma. The ion beam current Ar^{10+} is not presented due to the overlap with O^{4+}.

IV. DISCUSSION

The method of determining the cold electron temperature and ratio of low charge state ion densities in neon discharge can be applied to other elements as well. This requires identifying a set of suitable optical transitions fulfilling the following criteria: (i) the upper state of the observable transition is populated primarily by electron impact from the ground state of the neutral atom or ion, (ii) the contribution of other excitation channels, e.g., radiative and nonradiative decay from upper electronic states, is either negligible or can be estimated/measured, (iii) the branching ratio of the de-excitation process is well-known, and (iv) the energy-dependencies of the excitation cross sections populating the upper states are as different as possible, which allows calculating rate coefficient ratios for a number of excitation reaction pairs and using them to deduce the electron temperature (assuming a certain distribution function). As an example, Table V lists a set of transitions suitable for determining the cold electron temperature in argon plasmas.

The corresponding rate coefficient ratios for a Maxwellian electron population are shown in Fig. 6. All the given transitions are clearly visible in the emission spectrum of the JYFL 14 GHz ECRIS.

TABLE V. A set of Ar^{+} transitions suitable for determining the cold electron temperature.

Transition no.	Upper state	Lower state	Wavelength (nm)
1	$3s^2 3p^4(^1\mathrm{D})4p\ ^2\mathrm{P}^{o}_{3/2}$	$3s^2 3p^4(^1\mathrm{D})4s\ ^2\mathrm{D}_{5/2}$	427.753
2	$3s^2 3p^4(^3\mathrm{P})4p\ ^4\mathrm{D}^{o}_{5/2}$	$3s^2 3p^4(^3\mathrm{P})4s\ ^4\mathrm{P}_{3/2}$	442.600
3	$3s^2 3p^4(^1\mathrm{D})4p\ ^2\mathrm{F}^{o}_{7/2}$	$3s^2 3p^4(^1\mathrm{D})4s\ ^2\mathrm{D}_{5/2}$	460.957
4	$3s^2 3p^4(^3\mathrm{P})4p\ ^2\mathrm{P}^{o}_{1/2}$	$3s^2 3p^4(^3\mathrm{P})4s\ ^2\mathrm{P}_{3/2}$	465.790
5	$3s^2 3p^4(^3\mathrm{P})4p\ ^2\mathrm{D}^{o}_{5/2}$	$3s^2 3p^4(^3\mathrm{P})4s\ ^2\mathrm{P}_{3/2}$	487.986

The optical emission spectrum of argon contains several emission lines of Ar^{0}, Ar^{1+}, and Ar^{2+}, which allows determining their mutual densities using the estimated electron temperature. The argon example serves to demonstrate the steps required to obtain the cold electron temperature in different discharges, i.e., identifying suitable transitions, observing them in the emission spectrum, calculating the ratios of their rate coefficients for a chosen EED, and finally comparing the measured ratios of several transition pairs to the calculated ratios of the rate coefficients.

Several possible explanations for the higher-than-expected ion temperatures were listed previously,[3] the most prominent ones being (i) collisional energy transfer from the cold electron

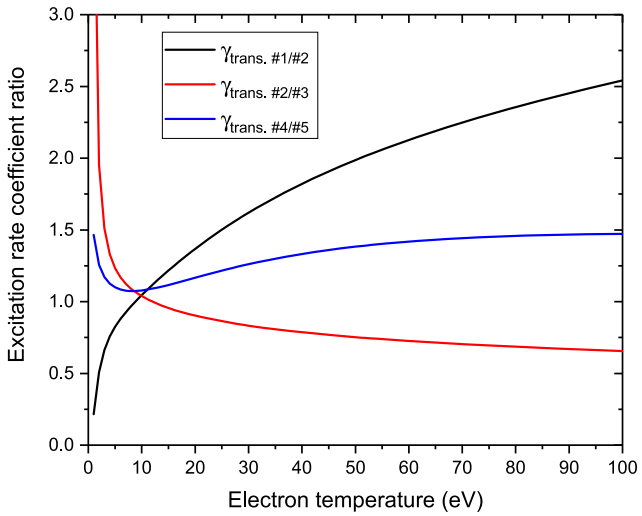

FIG. 6. Maxwellian rate coefficient ratios of the transitions suitable for determining the cold electron temperature in argon plasmas.

population to ions (electron drag) requiring long confinement, which is commensurate with the ions being confined electrostatically[20,21] and (ii) charge exchange between high charge state ions and neutral ($A^{q+} + B \rightarrow A^{(q-1)+} + B^{+}$) presumably heating the ions via the conversion of (electric) potential energy into kinetic energy due to Coulomb repulsion experienced by the reaction products and (iii) ionization in spatially varying electrostatic potential and subsequent conversion of the potential energy into kinetic energy.

It has been shown that the cumulative ion confinement time in ECRIS plasmas is sufficiently long[22,23] for the electron drag to be effective. Such gradual heating of the ions does not explain the 10 eV (order of magnitude) temperature of the Ar^{+}. Meanwhile, it can be estimated[1] that the energy gained by the Ar^{+} ions in the charge exchange reaction is on the order of 10 eV the precise energy depending on the charge state of the q+ ion. The contribution of charge exchange on the ion temperature can be assessed by comparing the probabilities of neutral gas ionization via charge exchange ($Ar^{0} + Ar^{q+} \rightarrow Ar^{+} + Ar^{(q-1)+}$) and electron impact ionization ($Ar^{0} + e \rightarrow Ar^{+} + 2e$), the energy exchange between the colliding particles being essentially zero in the latter process. The relative importance of the above reactions can be estimated by calculating the ratio of their rate coefficients

$$\frac{R_{ionz}}{R_{cex}} = \frac{n_n n_e \langle \sigma_{ionz} v_e \rangle}{n_n \sum n_i^q \langle \sigma_{cex,\,q} v_{i,q} \rangle}, \tag{3}$$

where n_n is the neutral density (canceling out), n_e is the electron density, σ is the cross section of either electron impact ionization or charge exchange (with a charge state q), v_e the electron velocity, and v_i the ion velocity. The total cross section of electron impact ionization of neutral argon is taken from Ref. 24, whereas the charge exchange cross sections and maximum energies of argon ions acquired through subsequent Coulomb repulsion are from Ref. 3. The electron impact cross section peaks well below 100 eV energy, i.e., it can be assumed that the cold electron population of the ECRIS plasma accounts for the majority of electron impact ionization of neutral argon and, therefore, the relative importance of the above reactions depends on the ratio of cold and hot electron densities. The ion densities of each charge state are estimated (ignoring their spatial distribution) from the charge state distribution (CSD) of the extracted beam.

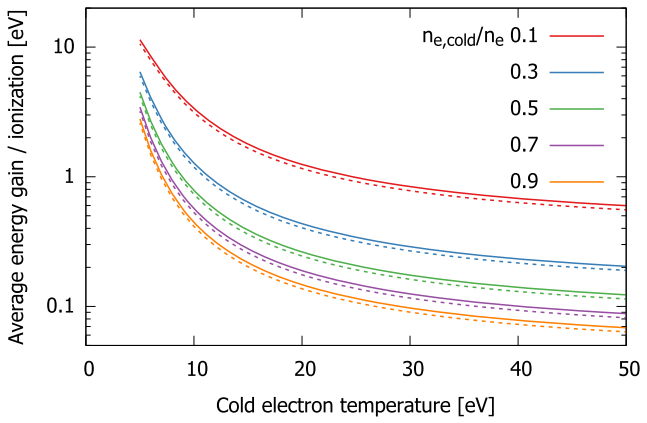

FIG. 7. The calculated average energy gain of the Ar^{+} ion ionized via electron impact or charge exchange ionization as a function of the cold electron temperature at different cold electron fractions. The charge state distribution of the confined ions was taken either from afterglow peak currents (solid) or from continuously extracted currents (dashed).

Figure 7 shows the estimated energy gain of a neutral Ar, ionizing to Ar^{+} either via charge exchange or electron impact ionization, as a function of the cold electron temperature with the cold electron fraction, $f_{e,cold} = N_{e,cold}/N_{e,total}$, ranging from 0.1 to 0.9 of the total electron population. From the rate coefficient analysis, it is concluded that (i) ionization by electron impact is the dominant ionization mechanism of argon in ECRIS plasmas, (ii) the charge state distribution has only a weak effect on the relative importance of the ionization pathways, and (iii) the observed 10 eV temperature of the 1+ ions cannot be explained by charge exchange unless the ions neutralize (e.g., in interaction with the plasma chamber wall) preserving the kinetic energy and experience several charge exchange ionization reactions.

V. FUTURE PLANS

Technical development of the high resolution spectrometer beyond its present capabilities aims at enabling time-resolved measurement of the line profiles of relatively strong emission lines such as 488 nm Ar^{+} and 553 nm Ar^{9+} with ms-level temporal resolution. The modifications of the OES setup required to achieve this include the following:

- Increasing the line-of-sight volume by upgrading the optics of the coupler connecting the ECRIS to the monochromator via the optical fiber.
- Systematic optimization of the circular slits of the monochromator to complete the process of removing the astigmatism, which improves the resolution of the device with increased throughput.
- Increasing the groove density of the diffraction grating, which improves the resolution and allows increasing the slit width (see the previous item).
- Converting the photomultiplier detection system to a high-sensitivity, high-speed CMOS or CCD sensor operating as a photon counter with appropriate cooling.
- Upgrading the data acquisition to the fast Field-Programmable Gate Array based system.

The experiments that become available after the ongoing upgrade include time-resolved measurement of the ion temperature either in pulsed operation mode of the ion source or with pulsed material injection, e.g., sputtering. Such experiments would probe the connection between the ion confinement time and ion temperature as well as the collisional energy exchange between different ion species in ECRIS plasmas relevant for understanding the gas mixing effect.

ACKNOWLEDGMENTS

The authors would like to thank the JYFL electrical and mechanical workshop for their help with technical issues and spectrometer calibration. The JYFL high resolution spectroscopy project has received funding from the European Union's Horizon 2020

research and innovation programme under Grant Agreement No. 654002 and the Academy of Finland under the Finnish Centre of Excellence Programme 2012–2017 (Nuclear and Accelerator Based Physics Research at JYFL, Project No. 213503) and the Academy of Finland Project funding (No. 315855).

REFERENCES

[1]R. Kronholm, T. Kalvas, H. Koivisto, and O. Tarvainen, "Spectroscopic method to study low charge state ion and cold electron population in ECRIS plasma," Rev. Sci. Instrum. **89**(4), 043506 (2018).
[2]R. Kronholm, M. Sakildien, D. Neben, H. Koivisto, T. Kalvas, O. Tarvainen, J. Laulainen, and P. Jones, AIP Conf. Proc. **2011**, 040014 (2018).
[3]R. Kronholm, T. Kalvas, H. Koivisto, J. Laulainen, M. Marttinen, M. Sakildien, and O. Tarvainen, Plasma Sour. Sci. Technol. **28**, 075006 (2019).
[4]K. L. Junck, M. L. Brake, and W. D. Getty, Plasma Chem. Plasma Process. **11**, 15 (1991).
[5]O. Tuske, L. Maunoury, J.-Y. Pacquet, C. Barué, M. Dubois, G. Gaubert, P. Jardin, N. Lecesne, P. Leherissier, F. Lemagnen, R. Leroy, M.-G. Saint-Laurent, and A. C. C. Villari, Rev. Sci. Instrum. **75**, 1529 (2004).
[6]H. Muto, Y. Ohshiro, S. Yamaka, S. Watanabe, M. Oyaizu, S. Kubono, H. Yamaguchi, M. Kase, T. Hattori, and S. Shimoura, Phys. Proc. **66**, 140 (2015) (the 23rd International Conference on the Application of Accelerators in Research and Industry - CAARI 2014).
[7]N. K. Bibinov, V. F. Bratsev, D. B. Kokh, V. I. Ochkur, and K. Wiesemann, Plasma Sour. Sci. Technol. **14**, 109 (2005).
[8]H. Koivisto, P. Heikkinen, V. Hänninen, A. Lassila, H. Leinonen, V. Nieminen, J. Pakarinen, K. Ranttila, J. Ärje, and E. Liukkonen, Nucl. Instrum. Methods B **174**, 379–384 (2001).
[9]R. W. Esplin, Opt. Eng. **19**, 623–627 (1980).
[10]G. Melin *et al.*, in *Proceedings of the 10th International Workshop on ECR Ion Sources, Knoxville, INS Report No. Conf.-9011136* (Oak Ridge National Laboratory, TN, USA, 1990), p.1.
[11]S. Runkel *et al.*, Rev. Sci. Instrum. **71**, 912 (2000).
[12]O. Tarvainen, P. Suominen, and H. Koivisto, Rev. Sci. Instrum. **75**, 3138 (2004).
[13]G. Melin, A. G. Drentje, A. Girard, and D. Hitz, J. Phys. Colloq. **86**, 4772–4779 (1999).
[14]A. Galatà, D. Mascali, L. Neri, and L. Celona, Plasma Sour. Sci. Technol. **25**, P045007 (2016).
[15]C. Petty, D. Goodman, D. Smith, and D. Smatlak, J. Phys. Colloq. **50**, C1-783–C1-789 (1989).
[16]C. C. Petty, D. L. Goodman, D. L. Smatlak, and D. K. Smith, Phys. Fluids B **3**, 705–714 (1991).
[17]A. G. Drentje, Nucl. Instrum. Methods Phys. Res., Sect. B **9**, 526 (1985).
[18]A. G. Drentje, A. Girard, D. Hitz, and G. Melin, Rev. Sci. Instrum. **71**, 623 (2000).
[19]O. Tarvainen, P. Suominen, T. Ropponen, T. Kalvas, P. Heikkinen, and H. Koivisto, Rev. Sci. Instrum. **76**(9), 093304 (2005).
[20]V. P. Pastukhov, Rev. Plasma Phys. **13**, 203–259 (1987).
[21]G. D. Shirkov, C. Mühle, G. Musiol, and G. Zschornack, Nucl. Instrum. Methods Phys. Res., Sect. A **302**, 1–5 (1991).
[22]D. Neben *et al.*, in *Proceedings of the ECRIS2016*, Busan, Korea, 2016, http://www.jacow.org, p. 128.
[23]M. Marttinen *et al.*, "Estimating ion confinement times from beam current transients in conventional and charge breeder ECRIS," Rev. Sci. Instrum. (these proceedings).
[24]H. Tawara and T. Kato, "Total and partial ionization cross sections of atoms and ions by electron impact," At., Data Nucl. Data Tables **36**, 167–353 (1987).